WATER RESOURCES RESEARCH, VOL. 37, NO. 5, PAGES 1173–1182, MAY 2001

Generation of stable microbubbles and their transport through porous media

Jiamin Wan, Srinivas Veerapaneni,[1] Fred Gadelle,[2] and Tetsu K. Tokunaga
Earth Sciences Division, Lawrence Berkeley National Laboratory, Berkeley, California

Abstract. Laboratory experiments were conducted to generate stable microbubbles and to measure their transport properties in porous media in order to evaluate their possible use in subsurface remediation. A mathematic model was developed as a special case of filtration theory for predicting microbubble transport in porous media. Several physical-chemical parameters were tested, including surfactant type, surfactant concentration, generation method, and pressure. A combination of an anionic surfactant and a hydrophobic nonionic surfactant was found to yield the highest concentrations of stable microbubbles (3×10^9 bubbles mL^{-1}) in the size range of 0.7 to 20 μm. The specific surface areas of the microbubble suspensions were in the range of 50 cm^2 mL^{-1}, and specific air volumes were >0.07 mL mL^{-1}. For 1 pore volume of injected bubble suspension, effluent recoveries of 100, 80, and 30% were achieved from columns of coarse (415–500 μm), medium (150–212 μm), and fine (53–106 μm) sands, respectively. Effluent recovery in the fine sand column increased to 63% following a 3 pore volume injection. Microbubble generation and injection under pressure were shown to minimize microbubble loss due to gas dissolution. Results from the modeling suggest that retention of microbubbles could be adequately described by filtration theory.

1. Introduction

Subsurface remediation of contaminants using air sparging relies on transfer of volatile contaminants into the injected air phase, which is then brought up to the surface into a treatment unit. Air sparging (biosparging) also increases the oxygen supply for promotion of in situ aerobic biodegradation of organic contaminants, though a related remediation technology, bioventing, is more specifically directed at this purpose. Commonly recognized problems associated with biosparging and bioventing are channeling of injected air up through a limited number of preferential pathways and limited radius of influence around air sparging injection wells. Preferential flow through fractures and macropores, a severe limitation of the conventional pump and treat approach to groundwater remediation, is also a primary concern in air sparging [e.g., *Johnson et al.*, 1993; *Leeson et al.*, 1995; *Baker et al.*, 1995; *Marley et al.* 1995]. To circumvent some of these problems, injection of microbubbles, also termed colloidal gas aphrons (CGA), is being considered as an alternative [*Jenkins et al.*, 1993; *Longe et al.*, 1995]. Although microbubble injection into groundwater is technically a more complicated procedure than air sparging, it may be more effective at distributing the gas phase over larger volumes and in providing more water-air interfacial area. For successful injection of microbubbles into groundwater, microbubbles should preferably be of smaller sizes to permit their transport through pore spaces and should have a long lifetime and a high resistance to coalescing. Potential advantages of microbubble injection include promoting aerobic conditions for bioremediation and contaminant sorption onto the microbubbles for subsequent removal with moving microbubbles. The gaseous interior of microbubbles serves as a sink for vapor phase partitioning and removal of volatile organic contaminants (microbubble sparging). Surfactants used to stabilize microbubbles can also be effective at emulsifying low-solubility nonaqueous phase liquids (NAPLs). Microbubbles also have small buoyant rise velocities, which are advantageous from the perspective of retaining suspension uniformity during injection and for permitting reasonable residence times in the subsurface environment. The initial distribution of microbubbles, immediately following injection, will probably exhibit the commonly unavoidable limitation of uncontrolled channeling along interconnected high-permeability pathways. However, during extended postinjection periods when groundwater flow is due largely to natural hydraulic potential gradients, buoyant rise of microbubbles may allow their efficient access to regions of lower permeability (enhanced transverse dispersion). All of the aforementioned factors suggest that subsurface microbubble contaminant fractionation might be developed into a practical cleanup technique. In addition, injection of nutrients or special enzymes into contaminated zones might be facilitated by their sorption onto mobile microbubbles.

In this paper, we describe the generation of microbubbles of small size (0.7–20 μm), high concentration, long lifetime, and high resistance to coalescing. We then provide information on stability and mobility of microbubbles injected into saturated sands. A model for microbubble transport in porous media is developed as a special case of filtration theory. Effects of dispersion, sorption, and bubble capture mechanisms are included in the model. However, effects of surface forces and dissolution of bubbles are not accounted for.

[1]Now at Advanced Environmental Technologies Division, Black and Veatch, Kansas City, Missouri.

[2]Now at Chevron Petroleum Technology Company, San Ramon, California.

Paper number 2000WR900331.
0043-1397/01/2000WR900331$09.00

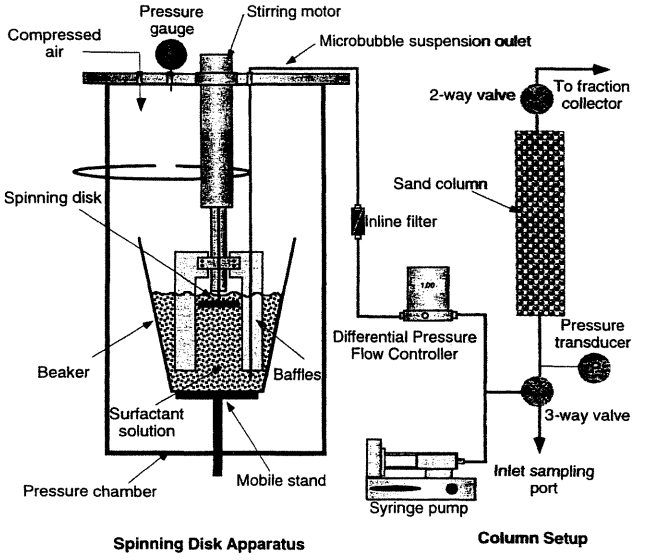

Figure 1. Spinning disk microbubble generator (based on the apparatus of *Sebba* [1994]) and microbubble transport column.

2. Microbubble Generation

2.1. Microbubble Generator

Microbubbles can be generated by mixing gas into a surfactant liquid, using disk impellers rotating at high speeds under pressures of 1 atm or greater. The spinning disk microbubble generator used in this study (Figure 1) is a modification based on the apparatus of *Sebba* [1994]. The generator is composed of a 5-cm-diameter disk mounted at the end of a shaft connected to an electrical motor, two vertical baffles, and a 4.5-L mixing beaker. The disk is mounted 2–3 cm below the surface of the surfactant solution and produces strong waves on the surface of the solution when rotating at high speeds (up to 16,000 rpm in our experiments). The waves hit the baffles and entrain air into the liquid. The entrained air subsequently breaks into microscopic bubbles that are stabilized by the surfactants [*Longe*, 1989; *Sebba*, 1985, 1994]. The microbubble generator is enclosed in a stainless steel chamber to generate microbubbles under pressure (up to 340 kPa). This design allows use of oxygen or other gases besides air and can generate suspensions with higher gas contents. In these experiments a known amount of surfactant is mixed with deionized (DI) water (1.5 L) in a 4.5-L beaker for 48 hours. The beaker is then placed on the stand in the pressure chamber. The chamber is tightly closed by the lid/spinning disk assembly and is pressurized using compressed gas. The beaker is subsequently raised using the mobile stand until the disk is positioned 2–3 cm below the surface of the solution. The microbubble suspension is then generated by spinning the disk for 10 min at a chosen speed. For producing smaller quantities of microbubble suspensions during initial screening comparisons of different surfactant mixtures an ultrasonic probe was used to generate 30 mL of microbubble solution [*Wheatley et al.*, 1994; *Wheatley and Singhal*, 1995]. The microbubble suspension was poured into separatory funnels to remove any excess solid surfactants present. After a 24-hour settling period the solid particles that sedimented to the bottom were removed, and the remaining solution containing microbubbles was used for further analysis. After generation of microbubbles and separation of solid particles the microbubble suspension was examined under a microscope to verify that the solution contained primarily microbubbles. Quantitative microbubble size analysis was done with a Coulter Multisizer IIe (Luton, England), using a 30-μm aperture for most tests. This aperture permitted size analyses in the 0.6- to 20-μm-diameter range, with a resolution of ± 0.1 μm. Other apertures were occasionally used to cover larger size ranges but with coarser resolution. All information on microbubble sizes and numbers provided in this study are based on measurements using the Multisizer IIe.

2.2. Factors Controlling Microbubble Concentration, Size Distribution, and Stability

2.2.1. Surfactant type and concentration. Batch experiments were conducted with several types and combinations of surfactants in order to generate stable and highly concentrated microbubble suspensions. A total of nine surfactants was tested: sorbitan monostearate (Span 60), sorbitan monopalmitate (Span 40), sodium dodecyl sulfate (SDS), polyoxyethylene sorbitan monooleate (Tween 80), octylphenol ethoxylate ether (Triton X100; Aldrich, Milwaukee, Wisconsin), sodium decyl sulfate (SDeS) (Acros Organics, Springfield, New Jersey), phosphate ester mixture (Rhodafac RE-960; Rhône-Poulenc, Cranbury, New Jersey), sodium lauryl ether sulfate (Witcolate ES270; Witco, Houston, Texas), and hexadecyl diphenyl oxide disulfonate (Dowfax 8390; Dow Chemicals, Midland, Michigan).

Bubbles produced with a single or a mixture of water-soluble surfactants, SDS, SDeS, RE-960, ES270, D8390, Tween 80, and Triton X100, had short life spans (less than an hour) and large sizes (30–100 μm). These bubbles also rapidly formed foam when left standing. Experiments conducted with hydrophobic surfactants (Span 60 and Span 40) yielded no bubbles. Stable microbubbles were generated by using the combinations of water-soluble surfactants and solid hydrophobic surfactants Span (e.g., SDS and Span 40, D8390 and Span 60, and Tween 80 and Span 60). This is consistent with the results reported by others. *Wheatley et al.* [1994] reported stable bubble generation using a combination of solid hydrophobic surfactants Span 60 and 40 and water-soluble Tween surfactants (Tween 20, 40, 60, 65, and 80). It should be noted that liquid hydrophobic surfactants Span 80 [*Wheatley et al.*, 1994] and undecanol and dodecanol (this work) do not form stable microbubbles. These results indicate that generation of stable microbubbles requires a solid hydrophobic surfactant in combination with a water-soluble surfactant. Such a combination stabilizes microbubbles by the formation of a solid-condensed monolayer at the gas-water interface. The tight packed monolayer can slow diffusive gas loss, and the surface tension of the mixed monolayer has been reported to approach zero [*Wang et al.*, 1996].

Among all the surfactant combinations examined, the combination of an anionic surfactant (SDS) and a nonionic surfactant (Span 60) was found to yield the highest concentrations and the most stable microbubbles, and such a combination was used throughout the rest of this study. Our results from the batch experiments also indicated that microbubble concentration increased with increasing the concentration of the nonsoluble Span 60. A concentration of 1 g L^{-1} of Span 60 was used through the rest of this work. The effect of SDS concentration on microbubble generation was also studied, and a concentration of 1 g L^{-1} was found to be optimal. At lower concentrations the amount of SDS was not sufficient to stabilize the microbubbles, and at higher concentrations, possible

micellization of SDS and/or solubilization of the Span 60 reduced the stability of microbubbles.

2.2.2. Spinning speed. Our tests showed that the concentration of generated microbubbles increased with increasing spinning speed of the disk impeller. Microbubble concentrations reached a plateau at around 13,000 rpm. At a speed of 10,000 rpm the temperature of the suspension rose from 21° to 25°C in 10 min. Higher temperatures at spinning speeds >13,000 rpm may have diminished the efficiency of microbubble generation. A speed of 13,000 rpm was used throughout the rest of this research.

2.2.3. Pressure. The influence of pressure on microbubble stability was tested since subsurface injection could subject microbubbles to a wide range of pressures. Significant loss of microbubbles was observed when the bubbles were subjected to pressures greater than that at which they were generated. This was caused by microbubble gas dissolution. For example, when microbubbles generated at 170 kPa were subjected to a pressure of 240 kPa, the number concentration of microbubbles declined from 1.6×10^9 to 1.2×10^9 number mL^{-1}, while the volume concentration decreased from 45×10^9 to 4×10^9 μm^3 mL^{-1}. The higher reduction in volume concentration suggests that most of the loss occurred in larger bubble size ranges, and it was also evident from the measured bubble size distribution. This is expected, as the larger microbubbles (4–15 μm) are more sensitive to the pressure increase. When subjected to a higher pressure of 310 kPa, further decrease in microbubble concentration (0.76×10^9 number mL^{-1} and 0.79×10^9 μm^3 mL^{-1}) was observed. Visual observation under a microscope confirmed that at this high pressure most of the bubbles had disappeared, leaving only small microbubbles around 1 μm and solid particles.

The effect of pressure on microbubble generation was also investigated. The concentrations of the microbubbles generated at three pressures are shown in Figure 2. Significantly higher concentrations were obtained at pressures of 225 and 310 kPa than at 135 kPa. The amount of dissolved gas in aqueous phase increases proportionally with increase in pressure of the adjacent gas phase, as expected from Henry's law. When the pressure is released, most of the gas transfers out of

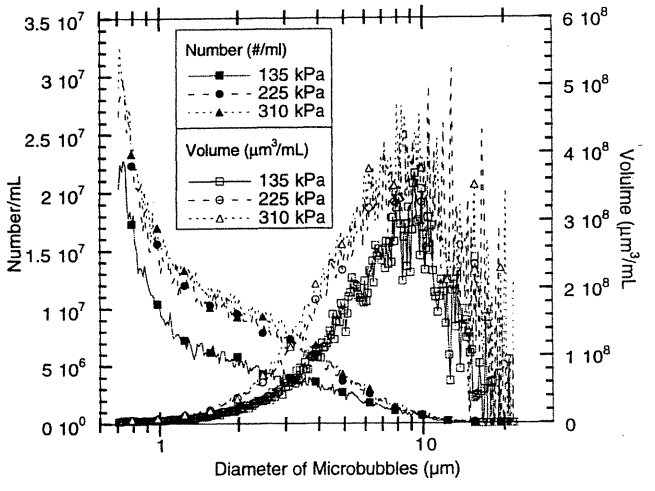

Figure 2. Concentration and size distribution of microbubbles generated at 3 pressures. (The curves represent data collected over 250 channels, each representing 1 size. To preserve clarity, only representative points are shown.)

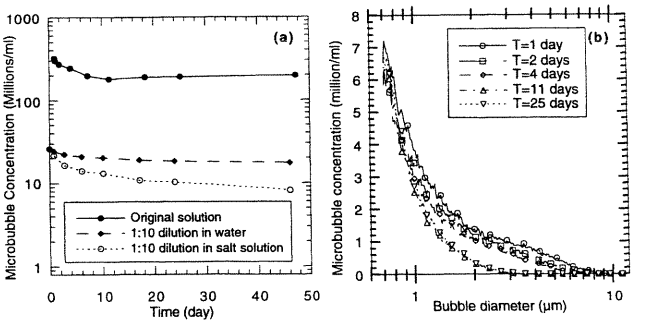

Figure 3. Stability of microbubbles over time: (a) concentration of microbubbles remaining in solution over time; Salt solution contained 1.0 mM NaCl and 0.5 mM $CaSO_4$ and (b) bubble size distribution of original suspension over time.

the aqueous phase in the form of bubbles, which are stabilized with the surfactants present in the solution, thereby increasing the number concentration of microbubbles generated at higher pressures.

2.2.4. Microbubble stability over time. The longevity of the microbubbles was tested by measuring the concentration and size distribution of the microbubbles over time. Three microbubble suspensions were tested: the original suspension, the original suspension diluted tenfold using DI water, and the original suspension diluted tenfold using a salt solution containing 1.0 mM NaCl and 0.5 mM $CaSO_4$. Figure 3a shows large numbers of microbubbles remained in the original as well as diluted suspensions even after 6 weeks. The bubble size distribution measurements over time revealed that significant loss of larger bubbles occurred over longer periods of time (Figure 3b). This is expected because the larger bubbles rise farther over time. As the bubbles rise, their size as well as rise velocity increases as the hydrostatic pressure decreases. Eventually, the bubbles rise to the surface and either form a foam or collapse at the air-water interface.

3. Microbubble Transport Through Porous Media

3.1. Theory

Microbubble transport in porous media may be treated as a special case of colloid transport. The one-dimensional transport equation with flow in the upward ($+z$) direction through a homogeneous medium is given by

$$R\frac{\partial C}{\partial t} = D\frac{\partial^2 C}{\partial z^2} - v_0\frac{\partial C}{\partial z} - k_a C, \qquad (1a)$$

where C $[L^{-3}]$ is the microbubble concentration, R is the retardation factor for local sorption equilibrium, t $[T]$ is time, v_0 $[L\ T^{-1}]$ is the pore water velocity, D $[L^2\ T^{-1}]$ is the dispersion coefficient ($D = \alpha_L v_0$, where α_L $[L]$ is the longitudinal dispersivity), and k_a $[T^{-1}]$ is the pseudo first-order rate coefficient for attachment. Assuming linear equilibrium adsorption, the retardation factor $R = 1 + \rho_{bulk} k_1/\varepsilon$, where ρ_{bulk} and ε are the dry bulk density and porosity of the porous medium, respectively, and k_1 $[M^{-1}\ L^3]$ is a distribution constant. More generally, microbubble gas dissolution also needs to be included. For short-term transport, without elevated pressure, dissolution may be assumed negligible. In this study, only microbubble retention by the porous media is considered.

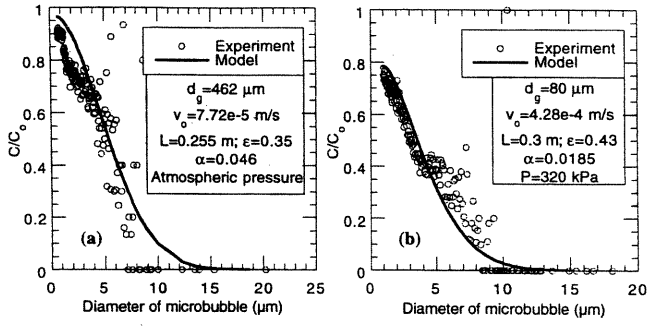

Figure 4. Normalized effluent concentrations of microbubbles, as a function of microbubble size for (a) medium sand and (b) fine sand. Other parameters are shown in the figures.

The following boundary conditions are appropriate for the experiments reported later in this study:

$$C(z, t) = 0 \qquad t = 0$$

$$C(z, t) = \begin{cases} C_0 & z = 0; \quad 0 < t \le t_0 \\ 0 & (z = 0; \quad t > t_0) \end{cases} \tag{1b}$$

$$\frac{\partial C(z, t)}{\partial z} = 0 \qquad z = L,$$

where C_0 $[L^{-3}]$ is the influent microbubble concentration and t_0 $[T]$ is the microbubble pulse injection duration time. The solution to (1a) and (1b) given by *Selim and Mansell* [1976] and *van Genuchten and Alves* [1982] is used to characterize microbubble transport, adjusting three parameters, D, R, and k_a, to fit the observed data. Two approaches were followed in modeling microbubble transport. In the first approach the three parameters, D, R, and k_a, were used as adjustable parameters to fit the data to (1). A nonlinear regression model based on a modified Levenberg-Marquardt method (routines RNLIN and R2LIN, International Mathematical and Statistical Libraries, Houston, Texas, 1997) is used to obtain a least squares estimate of the three parameters. For this method the total number of bubbles in the influent and effluent is considered.

In the second approach an estimate of the attachment coefficient, k_a, is obtained using filtration theory. Assuming that the microbubbles are rigid (which is a reasonable assumption since they are covered by a surfactant layer and behave as rigid spherical shells), the attachment rate coefficient, k_a, in (1) can be related to the filter coefficient, λ $[L^{-1}]$, used in the filtration theory as follows [*Yao et al.*, 1971]:

$$k_a = v_0\lambda = v_0\left[\frac{3}{2}\frac{(1-\varepsilon)\alpha\eta}{d_g}\right], \tag{2}$$

where ε is porosity and d_g is the diameter of the spherical grain of filter media (collector) diameter. The single-collector efficiency, η, in (2) is defined as the ratio of the rate at which particles strike the single collector to the rate at which particles flow toward the collector. The collision efficiency factor, α, is defined as the fraction of collisions that result in attachment of the particle to the collector. Under favorable surface interactions between the particle and the collector that result in a net attractive force, α approaches unity, while under unfavorable surface interactions resulting in a repulsive force barrier, α approaches zero. For the experiments reported in this study the microbubbles as well as the sand grains are negatively charged, and the value of α is expected to be low. The single-collector efficiency, η, can be determined by considering the different transport mechanisms such as inertial impact, diffusion, gravity, and electrostatic forces that cause the trajectories of particles to deviate from fluid streamlines and bring them into the proximity of the collector. Particles following streamlines may also be intercepted by a collector when the streamline passes within a distance of particle radius, by virtue of its size. Another possible removal mechanism, straining, occurs when particles in the suspension are larger than grain media pore size and results in cake formation. Filtration by straining is insignificant in our experiments because the sand grain sizes are far larger than our microbubbles. Filtration by inertial impact is also not possible because the density of microbubbles is less than that of water. Several models are available in the literature to calculate single-collector efficiency [*Tien*, 1989]. The underlying assumptions of all these filtration models are that the media grains and particles are spheres with uniform surface potentials and that filter grains are monodispersed and clean. In this study, the model for singles-collector efficiency proposed by *Rajagopalan and Tien* [1976] and by *Rajagopalan et al.* [1982] is used since it takes into account the effect of neighboring grains by incorporating *Happel*'s [1958] flow field hydrodynamic retardation caused by lubrication effects, and contribution of London-van der Waals attractive forces to particle deposition. On the basis of the analysis of particle trajectories around a spherical collector, *Rajagopalan and Tien* [1976] developed the following approximate expression for η as a function of several dimensionless numbers:

$$\eta = [4A_s^{1/3}N_{Pe}^{-2/3} + A_sN_{Lo}^{1/8}N_R^{15/8} + 0.00338A_sN_G^{1.2}N_R^{-0.4}], \tag{3a}$$

where

$$N_R = d_p/d_g, \tag{3b}$$

$$N_{Pe} = UD_c/[kT/(e\pi\mu d_p)], \tag{3c}$$

$$N_G = U_p/U, \tag{3d}$$

$$N_{Lo} = 4H/(9\pi\mu d_p^2U), \tag{3e}$$

$$A_2 = \frac{2(1-\gamma^5)}{2-3\gamma+3\gamma^5-2\gamma^6}, \tag{3f}$$

$$\gamma = (1-\varepsilon)^{1/3}, \tag{3g}$$

where d_p $[L]$ is the particle diameter, U $[L\ T^{-1}]$ is the approach velocity, k is the Boltzmann constant, T $[K]$ is temperature, μ $[M\ L^{-1}\ T^{-1}]$ is fluid viscosity. U_p $[L\ T^{-1}]$ is the particle settling velocity, and H $[M\ L^{-2}\ T^{-2}]$ is the Hamaker constant, usually assumed to be 10^{-20} J. In most filtration applications the density of particles is usually higher than that of the carrying fluid. This results in deposition due to settling of particles in the direction of the flow, which is usually in the downward direction $(-z)$. In this study, microbubbles are covered by a surfactant layer and behave as rigid spherical shells. The density of the gas within the microbubble is negligibly smaller than that of water and is ignored here. For such "particles," gravity-induced deposition due to buoyant rise may only occur in the upward direction $(+z)$, which is also the direction of our flow experiments. Under these considerations,

Table 1. Characteristics of Columns[a]

Pressure	Sand Grain Size, μm	$L \times D$, cm×cm	Porosity	Hydraulic Conductivity, m s^{-1}	Flow Rate, m d^{-1}
1 atm	415–500	25 × 2.54	0.36	7e–4	0.02–6.0
1 and 3 atm	150–212	25 × 2.54	0.37	1e–4	0.02–6.0 (1 atm) 37 (3 atm)
1 and 3 atm	53–106	25 × 2.54	0.40	5e–5	6.0 (1 atm) 37 (3 atm)

[a] L is column length and D is column inner diameter.

using Stokes' law to estimate buoyant rise velocity of the bubbles. U_p in (3c) is given by

$$U_p = g\rho_f d^2 p/18\mu_f, \tag{4}$$

where g $[L\ T^{-2}]$ is gravitational acceleration and ρ_f $[M\ L^{-3}]$ is density of the fluid. After estimating η from (3), calculation of attachment coefficient, k_a, requires estimation of the collision efficiency factor, α (see equation (2)). At steady state, neglecting dispersion, the one-dimensional filtration equation can be derived by integrating (1) over the length of the column ($z = 0$ *to* L) as follows:

$$C/C_0 = \exp(-\eta L), \tag{5}$$

where C and C_0 are the effluent and influent concentrations. For any given experiment the size of the microbubbles in the suspension is the only varying parameter in (5). Using α as the fitting parameter, experimental data of C/C_0 for various microbubble sizes at complete breakthrough can be fitted to (5). The modified Levenberg-Marquardt method is used to obtain a least squares estimate of α. Two such typical fits are shown in Figure 4a and 4b for experimental results from medium sand and fine sand (experiments described later). Note that even though the experimental conditions do not satisfy some of the model assumptions such as spherical monodispersed collectors, good qualitative agreement between model and experimental observations is evident for a values of 0.046 for medium sand and 0.0185 for fine sand. Transport of microbubbles larger than a few micrometers in size is severely limited, primarily because of capture during buoyant rise. Diffusive and buoyant capture will limit transport of smaller and larger microbubbles, respectively. Microbubbles in the 0.1 to 1 μm size range are the most mobile, owing to the lack of any dominant transport mechanism that brings the bubbles into the proximity of the collectors. The single-collector efficiency increases with decreasing collector size, as is evident from Figures 4a and 4b. The retention of bubbles is higher for the fine sand media. It should be noted that these general trends have also been previously considered for mineral colloids and microorganisms in groundwater [*McDowell-Boyer et al.*, 1986; *Harvey*, 1997].

With α estimated as described above, the k_a values could be calculated for each size class in the microbubble size distribution using (2) and (3). Using the k_a values estimated in this manner, the experimental data is fitted to (1) with D and R as adjustable parameters, using the modified Levenberg-Marquardt nonlinear regression model. Since k_a is dependent on the bubble size, (1) needs to be solved for each bubble size class. To calculate residuals at each observation, the total number concentration of bubbles in the effluent was estimated by summing the model predictions for effluent number concentrations for each bubble size range and then comparing them with the observed total concentration.

3.2. Experimental Methods for Transport Tests

Transport experiments were conducted in vertical sand columns under steady flow conditions to determine mobility and stability of microbubble in saturated porous media. The quartz sand (Accusand, Unimin Co., New Canaan, Connecticut) was separated into three grain sizes: 415–500 μm (coarse sand), 150–212 μm (medium sand), and 53–106 μm (fine sand). To remove fines, the sand was washed extensively with DI water, nitric acid, and sodium polyphosphate, following the procedure of *Wan et al.* [1994]. Columns were wet-packed to minimize entrapped air. The hydraulic properties of columns are listed in Table 1. For the experiments conducted at atmospheric pressure 1 pore volume of the microbubble suspension was injected from the bottom end of water-saturated columns (250 mm length, 25 mm diameter). Following the microbubble injection, a water flush (1.0 mM NaCl and 0.5 mM $CaSO_4$) was initiated at the same flow rate with a syringe pump. For the experiments conducted at elevated pressures, microbubbles were generated at pressures of 310 to 340 kPa and directly injected into the column. The setup for these experiments is shown in Figure 1. An in-line differential pressure flow controller regulated pressure. A 25-μm filter was used to prevent large bubbles from clogging up the top layers of porous medium. After injecting a predetermined amount of microbubble suspension (1 or 3 pore volumes), a bubble-free solution flush at the same flow rate was initiated. The pressure drop across the column was monitored using a differential pressure transducer (Validyne, Northridge, California). The influent microbubble concentration and size distribution were measured at the beginning as well as at the end of each experiment. Column effluent suspensions were collected with a fraction collector in 0.1 pore volume increments for microbubble size and concentration measurements (Multisizer IIe).

3.3. Results of Atmospheric Pressure Experiments

Column experiments were conducted at atmospheric pressures using coarse sand at flow rates varying from 1 to 0.01 pore volume per hour (PV h^{-1}). The breakthrough curves for all these experiments were similar and showed nearly conservative transport with little or no loss due to sorption and retention by sand media. Two typical experimental breakthrough curves for flow rates of 1 and 0.1 PV h^{-1} are shown in Figure 5a and 6, respectively. At a flow rate of 1 PV h^{-1}, microbubble transport is nearly conservative. At a lower flow rate of 0.1 PV h^{-1}, small loss of microbubbles is evident. The experimental results agree well with model predictions for α_L

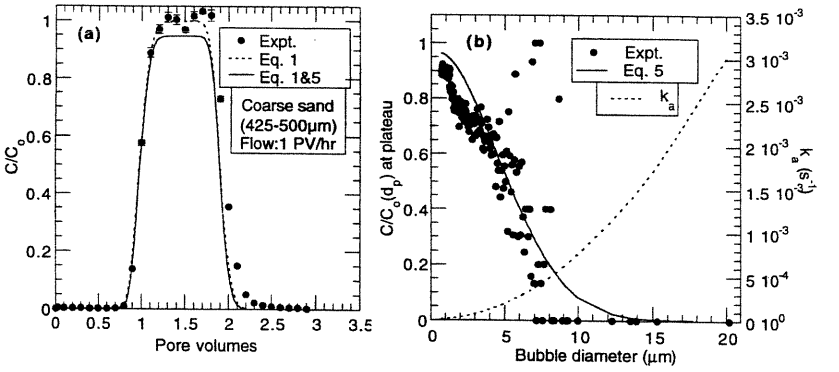

Figure 5. (a) Microbubble breakthrough curve for 1-PV pulse injection at atmospheric pressure into coarse sand (1 PV h^{-1}). Fitting parameters using equation (1) only are $\alpha_a = 1.15$ mm, $K_1 = 2 \times 10^{-5}$ kg^{-1} m^3, and $k_a = 6.37 \times 10^{-7}$ s^{-1}. Fitting parameters using equation (1) and (5) are $\alpha_L = 0.95$ mm and $k_1 = 2 \times 10^{-5}$ kg^{-1} m^3. (b) Normalized effluent concentration of microbubbles and k_a as a function of size ($\alpha = 2.38 \times 10^{-3}$).

values around 1 mm and k_1 values around 2 to 3×10^{-5} kg^{-1} m^3. The low k_1 value suggests little sorption of the bubbles onto the porous media. The small discrepancy between the two model predictions suggests that a good estimate of k_a value can be obtained from filtration theory. The effluent concentrations of microbubbles at the plateau normalized with the influent concentration for the experiment at 1 PV h^{-1} are shown as a function of the microbubble diameter in Figure 5b, along with the model predictions (equation)5)). A reasonable agreement between the model predictions and experimental data is obtained for attachment coefficient (α) values close to 2.4×10^{-3} (1 PV h^{-1}). An α value of 7.1×10^{-5} was obtained for the experiment at 0.1 PV h^{-1} (not shown). These low α values reflect very little microbubble attachment to sand grains. Also shown are the k_a values for each bubble size. Recall from (2) and (3) that k_a depends on bubble size through η. Note that the k_a values of smaller bubbles ($< \mu$m) are closer to the k_a value obtained from (1) alone. This is expected since the number concentration of these smaller microbubbles is high in the effluent, and thus they determine the number-based breakthrough curve shape.

Normalized effluent concentrations from experiments with

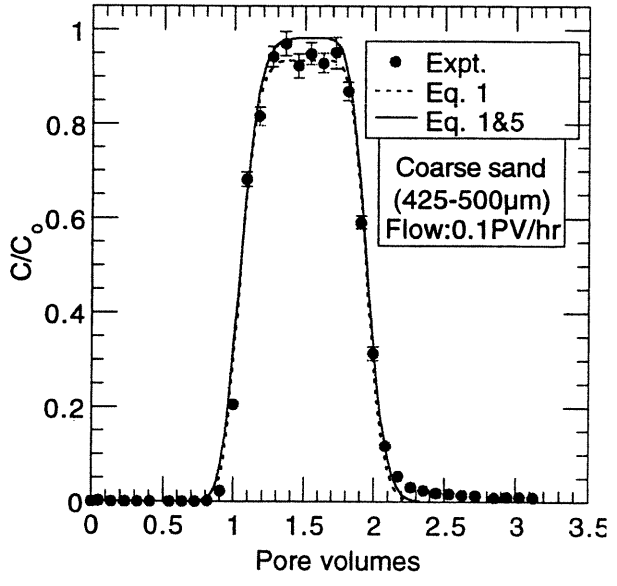

Figure 6. (a) Microbubble breakthrough curve for 1-PV pulse injection at atmospheric pressure into coarse sand (0.1 PV h^{-1}). Fitting parameters using equation (1) only are $\alpha_L = 1.08$ mm, $k_1 = 2.86 \times 10^{-5}$ kg^{-1} m^3, and $k_a = 1.84 \times 10^{-6}$ s^{-1}. Fitting parameters using equation (1) and (5) are $\alpha_L = 1.34$ mm, $k_1 = 2.91 \times 10^{-5}$ kg^{-1} m^3, and $\alpha = 7.1 \times 10^{-5}$.

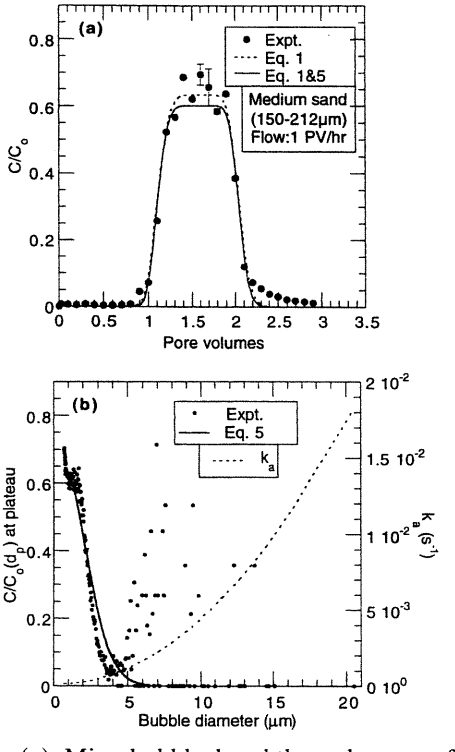

Figure 7. (a) Microbubble breakthrough curve for 1-PV pulse injection at atmospheric pressure into medium sand media (1 PV h^{-1}). Fitting parameters using equation (1) only are $\alpha_L = 1.06$ mm, $k_1 = 4.1 \times 10^{-5}$ kg^{-1} m^3, and $k_a = 1.38 \times 10^{-4}$ s^{-1}. Fitting parameters using equations (1) and (5) are $\alpha_L = 0.83$ mm and $k_1 = 4.22 \times 10^{-5}$ kg^{-1} m^3. (b) Normalized effluent concentration of microbubbles and k_a as a function of size ($\alpha = 7.42 \times 10^{-3}$).

medium grain sand (150–212 μm mesh size) at three different flow rates (1, 0.1, and 0.02 PV h^{-1}) are shown in Figures 7a, 8, and 9, along with model predictions. The normalized effluent concentrations in these experiments are lower than those from the coarse sand experiments. This is expected because the single-collector efficiency, as estimated from (3), increases with a decrease in collector grain size. In general, the model predictions agree reasonably well with experimental results. The small discrepancy between the two model predictions suggest that retention by sand media accounts for most of the bubble loss in the column. The bubble size dependence of effluent concentrations in the plateau region is qualitatively in good agreement with model predictions for α values in the range of 2×10^{-5} to 7.4×10^{-3}, suggesting little attachment (typical results are shown for 1 PV h^{-1} in Figure 7b). At lower flow rates the breakthrough curves are slightly asymmetrical (e.g., Figure 9). The reason for the asymmetry is not clear, though it may partly be attributed to the bubble size distribution effect on dispersion. Comparison of the maximum C/C_0 values in Figures 7a to 9 indicates that the column retention decreased with decrease in flow rate. However, single-collector efficiency is expected to increase with decrease in flow rate (equation (3)). The reason for this discrepancy is not clear, though it is likely that the higher pressure needed to maintain higher flow rates might have caused dissolution of some microbubbles.

Results from an experiment conducted with fine grain sand at a flow rate of 1 PV h^{-1} are shown in Figure 10a, along with model predictions. Model predictions based on filtration theory (equations (1) and (5)) do not agree with experimental observations. As expected, owing to the small grain size, the model predicts effluent concentrations that are significantly lower when compared to previous experiments with coarse and medium sand grain sizes. Recall that the single-collector efficiency, η, increases with decreasing grain size. The effluent concentrations at plateau, as a function of bubble sizes, do not agree with model predictions (Figure 10b). The steep decline in normalized bubble concentration with size indicates significant loss of bubbles due to mechanisms other than filtration, such as bubble dissolution caused by higher pressures needed to force the suspension through the fine sand. To limit bubble loss due to dissolution, several experiments were conducted with microbubbles generated under pressure and injected directly into the column at the same pressure. Results from these experiments are discussed in section 3.4.

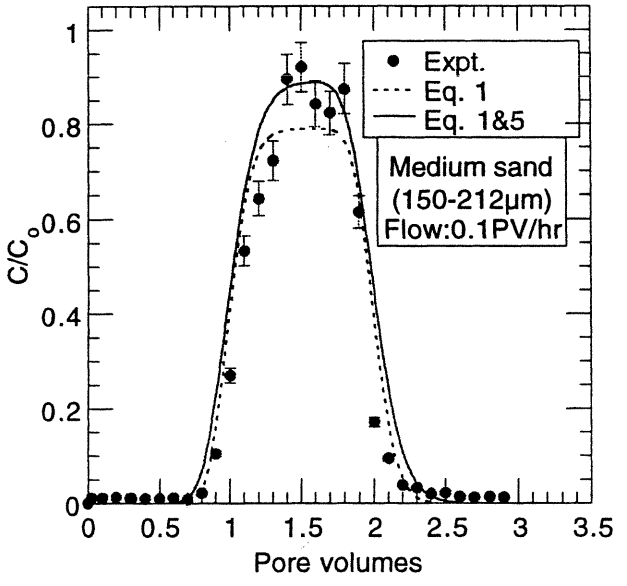

Figure 8. Microbubble breakthrough curve for 1-PV pulse injection at atmospheric pressure into medium sand (0.1 PV h^{-1}). Fitting parameters using equation (1) only are α_L = 1.92 mm, $k_1 = 2.1 \times 10^{-5}$ kg^{-1} m^3, and $k_a = 7.3 \times 10^{-6}$ s^{-1}. Fitting parameters using equation (1) and (5) are α_L = 0.32 mm, $k_1 = 2.38 \times 10^{-5}$ kg^{-1} m^3 and $\alpha = 2.45 \times 10^{-4}$.

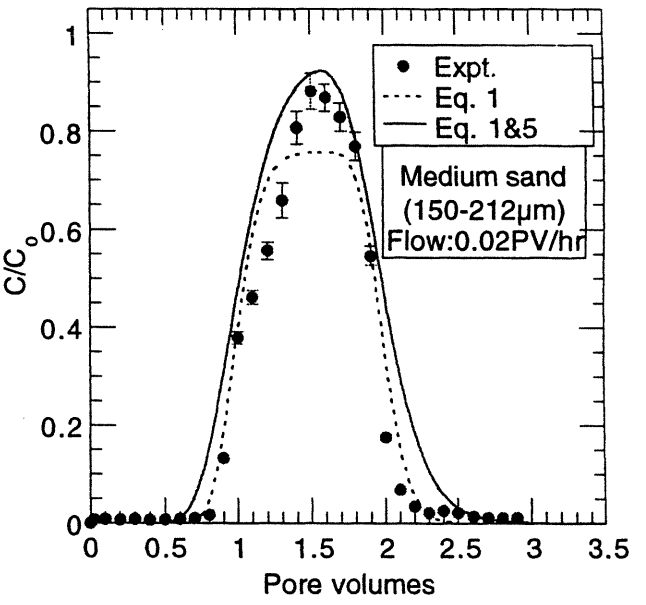

Figure 9. Microbubble breakthrough curve for 1-PV pulse injection at atmospheric pressure into medium sand media (0.02 PV h^{-1}). Fitting parameters using equation (1) only are α_L = 2.48 mm, $k_1 = 2.14 \times 10^{-5}$ kg^{-1} m^3, and $k_a = 1.75 \times 10^{-6}$ s^{-1}. Fitting parameters using equation (1) and (5) are α_L = 6.6 mm, $k_1 = 3 \times 10^{-5}$ kg^{-1} m^3, and $\alpha = 1.96 \times 10^{-5}$.

3.4. Results From Elevated Pressure Experiments

Microbubble breakthrough curves for five experiments conducted at elevated pressure are shown in Figure 11a. In these experiments, microbubbles were generated at 310 to 340 kPa in the pressure chamber and were then directly injected into columns. Results from these replicate experiments show that reasonable reproducibility is possible. However, some degree of scatter is inevitable due to the limitations of the flow controller and the problems associated with maintaining the same pressure during an experiment and between experiments. As with previous experiments, 1 pore volume of the microbubble suspension was injected from the bottom end of water-saturated columns followed by a microbubble-free salt solution flush at the same flow rate. However, the influent flow rates (5 PV h^{-1}, 37 m d^{-1}) for these experiments were significantly higher than those conducted at atmospheric pressure (0.01 to 1 PV h^{-2}, 0.06 to 6 m d^{-1}). As in experiments conducted at atmospheric pressure, some loss of microbubbles due to retention by porous media and dissolution is evident. Model predictions for one set of data (solid circles) are also shown, and good agreement with observed values is evident. The effluent concentrations at plateau as a function of bubble sizes agree well with model predictions for an α value of 7.2×10^{-3}

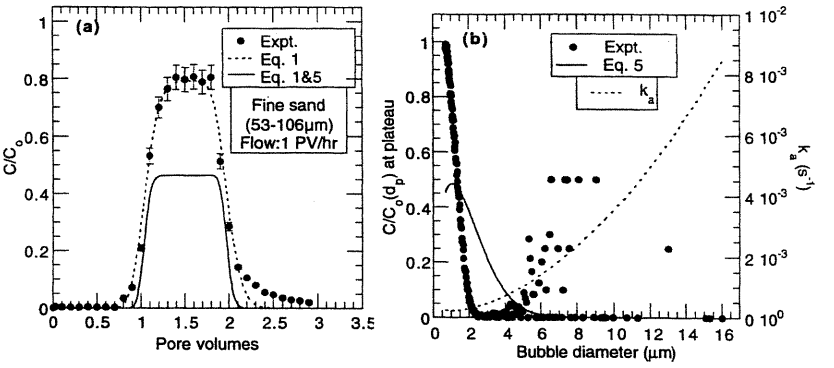

Figure 10. (a) Microbubble breakthrough curve for 1-PV pulse injection at atmospheric pressure into fine sand (1 PV h^{-1}). Fitting parameters using equation (1) only are $\alpha_L = 1.95$ mm, $k_1 = 3.56 \times 10^{-5}$ kg^{-1} m^3, and $k_a = 7 \times 10^{-5}$ s^{-1}. Fitting parameters using equation (1) and (5) are $\alpha_L = 0.42$ mm and $k_1 = 3.1 \times 10^{-5}$ kg^{-1} m^3. (b) Normalized effluent concentration of microbubbles and k_a as a function of size ($\alpha = 4.46 \times 10^{-3}$).

(Figure 11b). This value of α is higher than that obtained for experiments conducted at atmospheric experiments.

Results from duplicate experiments conducted with fine grain sand are shown in Figure 12a. Also included was the breakthrough curve for a nonreactive tracer (NaCl solution). As was the case with the experiments conducted at atmospheric pressure, the effluent concentrations are significantly lower when compared to those from experiments with medium grain sizes, and could be attributed to higher retention by the smaller pores of the fine sand as well as greater dissolution. It is interesting to note that breakthrough appears to have occurred twice. The first breakthrough, characterized by a small C/C_0, occurred at about the same time as that of a nonreactive tracer. The second breakthrough, characterized by C/C_0 values of ~75%, was significantly retarded compared to that of the tracer. Microbubble size distribution measurements indicated that the first breakthrough was primarily due to the passage of a small number of microbubbles with diameters <1 μm, while the effluent during the second breakthrough contained microbubbles with size distribution similar to those present in the influent (Figure 12b). To fit (5) to the C/C_0 value at first breakthrough, α values higher than 1 are needed. The cause of this initial breakthrough of small bubbles is not clear, though it is reproducible in both the experiments shown in Figure 12a as well as in a continuous injection experiment discussed next.

Experiments discussed so far involved injection of a pulse of 1 pore volume microbubbles into the column followed by a flush with bubble-free solution. In such experiments, the influent microbubbles are essentially exposed to clean porous medium. As discussed earlier, some retention of microbubbles occurred in medium grain sand, while significant amount of bubbles were retained in fine sand media. To study the effect of these retained bubbles on the transport of subsequently injected microbubbles, several continuous injection experiments were conducted with medium and fine sands. In these experiments, 3 PV of microbubbles were injected, followed by a flush with bubble-free salt solution. The normalized effluent concentrations are shown in Figure 13. Also included are pressure changes during the course of these experiments. The breakthrough for the medium sand occurred at concentrations close to that of influent, as was the case with pulse injection experiments. However, as the microbubble injection continued, the effluent concentration increased, with values of C/C_0 above 1 after ~2 pore volumes eluted. This is followed by slight decreases and increases with $C/C_0 > 1$ at around 3 PV. The high values of C/C_0 suggest that some of the previously re-

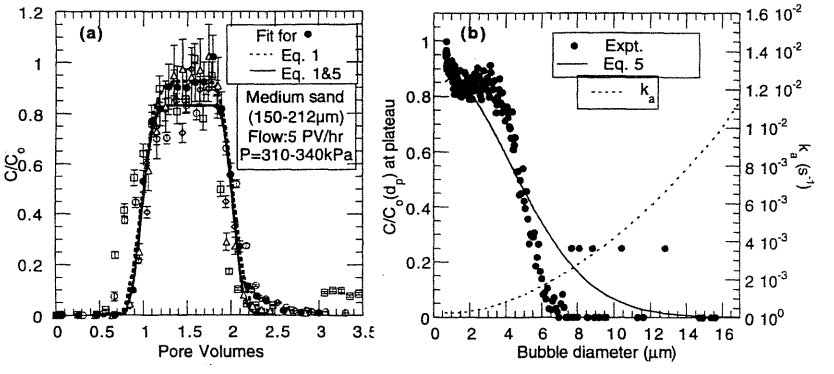

Figure 11. (a) Microbubble breakthrough curve for 1-PV pulse injection at 310–340 kPa into medium sand media (5 PV h^{-1}). Fitting parameters (for data shown as solid circles) using equation (1) only are $\alpha_L = 2.01$ mm, $k_1 = 1.24 \times 10^{-4}$ kg^{-1} m^3, and $k_a = 1.75 \times 10^{-6}$ s^{-1}. Fitting parameters using equation (1) and (5) are $\alpha_L = 1.3$ mm and $k_1 = 1.86 \times 10^{-5}$ kg^{-1} m^3. (b) Normalized effluent concentration of microbubbles and k_a as a function of size ($\alpha = 7.24 \times 10^{-3}$).

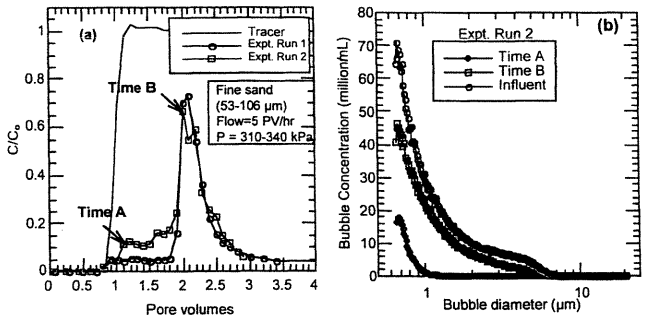

Figure 12. (a) Microbubble breakthrough curves for 1-PV pulse injection at elevated pressure into columns packed with fine sand. Duplicate runs are shown, along with the inert solute tracer breakthrough from one run. (b) Microbubble size distributions at two breakthrough times (A and B in Figure 12a), along with the influent microbubble size distribution.

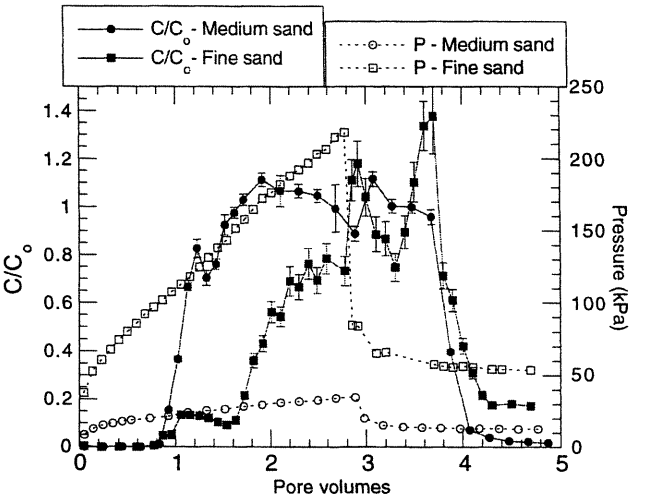

Figure 13. Normalized effluent concentrations through medium and fine sand columns. Three pore volumes of microbubbles have been injected, followed by flushing. Influent pressures are also shown.

tained bubbles are reentrained. The increase in pressure during this stage suggests blocking of some pores by microbubble aggregates. At the completion of 3-PV injection a sudden drop in pressure was observed, and may be attributed to the switching of pumps to inject bubble-free solution. In our system, disturbances in flow and pressure are unavoidable during switching of influent sources. We believe that this disturbance permits detachment of some microbubbles within the column, hence reduced hydraulic resistance and diminished inlet pressures. This process is consistent with the observed temporary increase in effluent C/C_0 shortly following the switching of sources.

Results for the 3-PV injection in fine sand column are also shown in Figure 13. As with the pulse input experiments, two breakthroughs were observed. The initial breakthrough, characterized by a small C/C_0, contained only smaller bubbles. The second breakthrough had a C/C_0 of ~80% and a microbubble size distribution similar to that of the influent. After the second breakthrough occurred, results were similar to those of the medium sand experiment. Normalized effluent concentrations higher than 1 were observed after 3 and also after 4 pore volumes injection. The effluent concentration profile indicates some retention of bubbles as well as their reentrainment. However, pressure increase is significantly higher in fine sand compared to that of medium sand. This is expected since fewer bubbles are needed to block the small pores in the fine sand columns compared to the larger pores present in medium grain sand columns.

4. Conclusions and Implications

Generation of long lasting and stable microbubble suspensions is accomplished using a mixture of an anionic surfactant (sodium dodecyl sulfate) and a hydrophobic nonionic surfactant (sorbitan monostearate, Span 60). These microbubbles ranged from 0.7 to 20 μm in size, with concentrations up to 3×10^9 bubbles mL^{-1}, specific volumes up to 70×10^9 μm mL^{-1}, and specific surface area up to 50 cm^2 mL^{-1}. The lifetime of

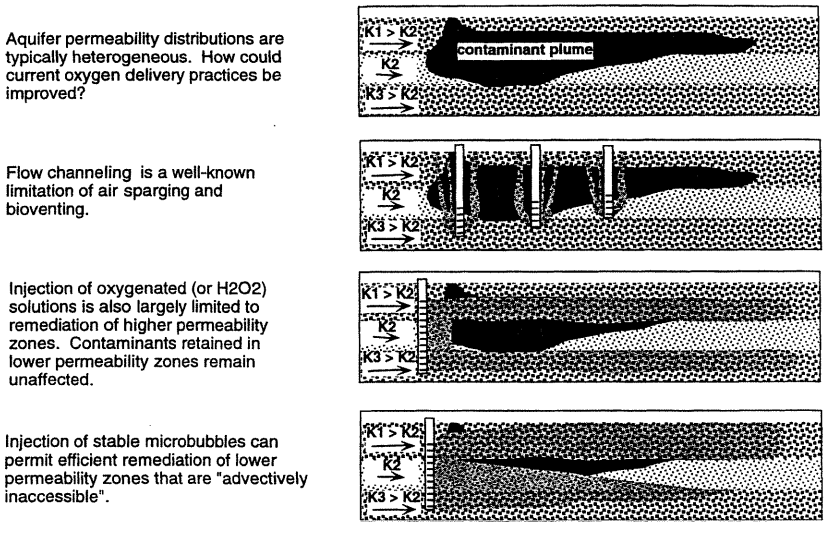

Figure 14. Surfactant stabilized microbubbles that might enhance delivery of oxygen by buoyant rise into advectively less accessible zones for in situ remediation.

these microbubbles can exceed 7 weeks. Column experiments involving injection of microbubbles into sand media of three size ranges were conducted to evaluate transport characteristics of the microbubbles. Complete microbubble recovery was obtained from effluents of the coarse (415–500 μm) sand. Microbubble recovery in effluents decreased to 80% and 30% in the medium (150–212 μm) and fine (53–103 μm) sands, respectively. Recoveries in the fine sand column increased to 63% when a longer, 3 pore volume injection was applied. The problem of microbubble gas dissolution was partially compensated for by microbubble generation and injection under higher pressures.

Transport characteristics of microbubbles in saturated sand columns were adequately described using filtration theory. The low values of attachment coefficient (α) needed to fit the experimental results with model predictions suggest that the surface interactions between the sand grains and bubbles are not favorable for deposition. Under such unfavorable surface interactions, microbubbles can travel significant distances in subsurface environments. Results from continuous injection experiments suggest that the role of retained bubbles in removing subsequently injected bubbles (ripening effect) on the transport of microbubbles is negligible in medium sand and that continued injection is possible with little increase in pressure. While the ripening effect was also observed to be limited in fine sands, significantly higher pressures are needed to maintain the flow rate.

These results indicate that microbubble suspensions can be used as air/oxygen carriers in some subsurface environments, especially when generated under elevated pressure. In such a case, substantial increases in oxygen delivery can be achieved. Potential advantages of microbubble suspension injection include enhanced delivery of oxygen, and buoyant rise into advectively less accessible regions (Figure 14). We identified some restrictive conditions under which microbubble injection might be effective. Our tests indicate that microbubbles ≈ 1 μm size will have favorable mobility in regions with permeabilities higher than 5×10^{-12} m^2. Thus microbubble injection and mobility are not expected to be effective in moderate and low permeability media. Filtration also generally imposes severe limits for both much larger and much smaller size microbubbles. Dissolution of microbubbles upon exposure to elevated pressure can be diminished by generation under high pressure.

Acknowledgments. This work was supported by Environmental Management Science Program of U.S. Department of Energy (contract DE-AC03-76SF00098). We thank Clay Radke (University of California, Berkeley) for helpful discussion, Mark Yahnke (LBNL) for technical support during the initial phase of this work, and Terry Hazen (LBNL) for the helpful internal review of this manuscript. We greatly appreciate the very helpful review comments and suggestions provided by the Associate Editor Stephen Silliman.

References

Baker, R. S., M. E. Hayes, and S. H. Frisbie, Evidence of preferential vapor flow during in situ air sparging, in *In Situ Aeration: Air Sparging, Bioventing, and Related Remediation Processes*, edited by R. E. Hinchee, R. N. Miller, and P. C. Johnson, pp. 63–73, Battelle Press, Columbus, Ohio, 1995.

Happel, J., Viscous flow in multiparticle systems: Slow motion of fluids relative to beds of spherical particles, *AIChE J.*, *4*, 197–201, 1958.

Harvey, R. W., Microorganisms as tracers in groundwater injection and recovery experiments: A review, *FEMS Microbiol. Rev.*, *20*, 461–472, 1997.

Jenkins, K. B., D. L. Michelsen, and J. T. Novak, Application of oxygen microbubbles for in slitu biodegradation of p-xylene-contaminated groundwater in a soil column, *Biotechnol. Prog.*, *9*, 394–400, 1993.

Johnson, R. L., P. C. Johnson, D. B. McWhorter, R. E. Hinchee, and I. Goodman, An overview of in situ air sparging, *Ground Water Monit. Rem.*, *13*, 127–135, 1993.

Leeson, A., R. E. Hinchee, G. L. Headington, and C. M. Vogel, Air chnannel distribution during air sparging: A field experiment, in *In Situ Aeration: Air Sparging, Bioventing, and Related Remediation Processes*, edited by R. E. Hinchee, R. N. Miller, and P. C. Johnson, pp. 215–222, Battelle Press, Colombus, Ohio, 1995.

Longe, T. A., Colloidal gas aphrons: Generation, flow characterization and application in soil and groundwater decontamination, Ph.D. dissertation, Va. Polytech. Inst. and State Univ., Blacksburg, 1989.

Longe, T. A., J. X. Bouillard, and D. L. Michelsen, Use of microbubble dispersion for soil scouring, in *In Situ Aeration: Air Sparging, Bioventing, and Related Remediation Processes*, edited by R. E. Hinchee, R. N. Miller, and P. C. Johnson, pp. 511–518, Battelle Press, Columbus, Ohio, 1995.

Marley, M. C., C. J. Bruell, and H. H. Hopkins, Air sparging technology: A practical update, in *In Situ Aeration: Air Sparging, Bioventing, and Related Remediation Processes*, edited by R. E. Hinchee, R. N. Miller, and P. C. Johnson, pp. 31–37, Battelle Press, Columbus, Ohio, 1995.

McDowell-Boyer, L. M., J. R. Hunt, and N. Sitar, Particle transport through porous media, *Water Resour. Res.*, *22*, 1901–1921, 1986.

Rajagopalan, R., and C. Tien, Trajectory analysis of deep-bed filtration with the sphere-in-cell porous media model, *AIChE J.*, *22*, 523–533, 1976.

Rajagopalan, R., C. Tien, R. Pfeffer, and G. Tardos, Letter to the editor, *AIChE J.*, *28*, 871–872, 1982.

Sebba, F., An improved generator for micron-sized bubbles, *Chem. Ind.*, 91–92, 1985.

Sebba, F., *Foams and Biliquid Foams—Aphrons*, John Wiley, New York, 1994.

Selim, H. M., and R. S. Mansell, Analytical solution of the equation for transport of reactive solutes through soils, *Water Resour. Res.*, *12*, 528–532, 1976.

Tien, C., *Granular Filtration of Aerosols and Hydrosols*, Butterworths London, 1989.

van Genuchten, M. T., and W. J. Alves, Analytical solutions of the one-dimensional convective-dispersive salute transport equation, *Tech. Bull. 1661*, U.S. Dep. of Agric., Washington, D.C., 1982.

Wan, J., Wilson, J. L., and T. L. Kieft, Influence of the gas-water interface on transport of microorganisms through unsaturated porous media, *Appl. Environ. Microbiol.*, *60*, 509–516, 1994.

Wang, W., C. C. Moser, and M. A. Wheatley, Langmuir trough study of surfactant mixtures used in production of a new and contrast agent consisting of stabilized microbubbles, *J. Phys. Chem.*, *100*, 13,815–13,821, 1996.

Wheatley, M. A., and S. Singhal, Structural studies on stabilized microbubbles: Development of a novel contract agent for diagnostic ultrasound, *React. Polym.*, *25*, 157–166, 1995.

Wheatley, M. A., P. Shen, S. Singhal, and B. B. Goldberg, Surfactant-stabilized microbubble mixtures, process for preparing and methods of using the same, Patent 5,352,436, U.S. Pat. Off., Washington, D.C., 1994.

Yao, K.-M., M. T. Habibian, and C. R. O'Melia, Water and wastewater filtration: Concepts and applications, *Environ. Sci. Technol.*, *5*, 1105–1112, 1971.

F. Gadelle, Chevron Petroleum Technology Company, 6001 Bollinger Canyon Road, San Ramon, CA 94853. (fgad@chevron.com)

T. K. Tokunaga, Earth Sciences Division, Lawrence Berkeley National Laboratory, MS 90-1116, Berkeley, CA 94720. (tktokunaga@lbl.gov)

S. Veerapaneni, Advanced Environmental Technologies Division, Black and Veatch, 8400 Ward Parkway, Kansas City, MO 64114. (VeerapaneniS@lbv.com)

J. Wan, Earth Sciences Division, Lawrence Berkeley National Laboratory, MS 90-1116, Berkeley, CA 94720. (jmwan@lbl.gov)

(Received April 21, 2000; revised October 13, 2000; accepted October 17, 2000.)